

Interacting Stress Intensity Factors of Multiple Elliptical-Holes and Cracks Under Far-Field and Arbitrary Surface Stresses

Wei Yi¹, Qiuhua Rao^{1,*}, Wei Zhu², Qingqing Shen¹, Zhuo Li¹
and Wenbo Ma³

¹ School of Civil Engineering, Central South University, Changsha, Hunan 410083, China

² School of Mathematics and Computational Science, Xiangtan University, Xiangtan, Hunan 411105, China

³ College of Civil Engineering and Mechanics, Xiangtan University, Xiangtan, Hunan 411105, China

Received 26 February 2021; Accepted (in revised version) 2 May 2021

Abstract. Calculating interacting stress intensity factors (SIFs) of multiple elliptical-holes and cracks is very important for safety assessment, stop-hole optimization design and resource exploitation production in underground rock engineering, e.g., buried tunnels, deep mining, geothermal and shale oil/gas exploitation by hydraulic fracturing technology, where both geo-stresses and surface stresses are applied on buried tunnels, horizontal wells and natural cracks. However, current literatures are focused mainly on study of interacting SIFs of multiple elliptical-holes (or circular-holes) and cracks only under far-field stresses without consideration of arbitrary surface stresses. Recently, our group has proposed a new integral method to calculate interacting SIFs of multiple circular-holes and cracks subjected to far-field and surface stresses. This new method will be developed to study the problem of multiple elliptical-hole and cracks subjected to both far-field and surface stresses. In this study, based on Cauchy integral theorem, the exact fundamental stress solutions of single elliptical-hole under arbitrarily concentrated surface normal and shear forces are derived to establish new integral equation formulations for calculating interacting SIFs of multiple elliptical-holes and cracks under both far-field and arbitrary surface stresses. The new method is proved to be valid by comparing our results of interacting SIFs with those obtained by Green's function method, displacement discontinuity method, singular integral equation method, pseudo-dislocations method and finite element method. Computational examples of one elliptical-hole and one crack in an infinite elastic body are given to analyze influence of loads and geometries on interacting SIFs. Research results show that when $\sigma_{xx}^{\infty} \geq \sigma_{yy}^{\infty}$, there appears a neutral crack orientation

*Corresponding author.
Email: raoqh@csu.edu.cn (Q. Rao)

angle β_0 (without elliptical-hole's effect). Increasing $\sigma_{xx}^\infty/\sigma_{yy}^\infty$ and b/a (close to circular-hole) usually decreases β_0 of K_I and benefits to the layout of stop-holes. The surface compressive stresses applied onto elliptical-hole (n) and crack (p) have significant influence on interacting SIFs but almost no on β_0 . Increasing n and p usually results in increase of interacting SIFs and facilitates crack propagation and fracture networks. The elliptical-hole orientation angle (α) and holed-cracked distance (t) have great influence on the interacting SIFs while have little effect on β_0 . The present method is not only simple (without any singular parts), high-accurate (due to exact fundamental stress solutions) and wider applicable (under far-field stresses and arbitrarily distributed surface stress) than the common methods, but also has the potential for the anisotropic problem involving multiple holes and cracks.

AMS subject classifications: 74A10, 78B05

Key words: Interacting stress intensity factors, multiple elliptical-holes and cracks, far-field stresses, arbitrary surface stresses, integral equation method.

1 Introduction

In underground rock engineering such as buried tunnels, deep mining, geothermal and shale oil/gas exploitation by hydraulic fracturing technology, both the geo-stresses and surface stresses (e.g., seepage pressure) are applied onto the buried tunnels, horizontal wells and natural cracks [1–4]. In addition, buried tunnels are usually designed in elliptical cross-sections for the improving stability of tunnels [5,6] and horizontal wells actually presents the form of elliptical-holes due to the long-term action of gravity stresses [7,8]. Under the external loads, the elliptical-holes have probability of facilitating or restraining initiation and propagation of natural cracks existing in the rock mass, since the different layouts of elliptical-holes can enlarge or reduce interacting stress intensity factors (SIFs). Consequently, calculating interacting SIFs of multiple elliptical-holes and cracks under complex loads plays an important role in safety assessment, stop-hole optimization design and resource exploitation production in underground rock engineering.

Up to now, many methods are available for calculating interacting SIFs of circular-holes and cracks under far-field loadings. For instance, Laurent series expansion method [9,10] and Green's function method [11,12] were used for one circular-hole and one crack, and boundary collection method [13], volume integral equation method [14], singular integral equation method [15] and boundary integral method [16,17] were adopted for the problem of multiple circular-holes and cracks. Very few literatures are reported for surface stresses applied on the circular-holes and cracks, especially for arbitrary surface stresses. In addition, there are also some methods for calculating interacting SIFs of elliptical-holes and cracks. For example, perturbation method [18], singular integral equation method [19] and boundary element method [20] were applied for solving the problem of one elliptical-hole and one crack, one elliptical-hole and multiple cracks, multiple elliptical-holes and one crack, respectively. For more complicated

problem of multiple elliptical-holes and cracks under far-field loadings, Yan [21] proposed a displacement discontinuity method to approximately calculate interacting SIFs based on the displacement discontinuity elements of nonsingular constant and crack-tips. Yang and Soh [22] presented a special finite element method with hybrid-type and semi-analytic-type elements for calculating interacting SIFs, where the solution accuracy and computation efficiency are difficult to be satisfied simultaneously. Han and Wang [23] developed a pseudo-dislocations method to obtain interacting SIFs within high accuracy by transforming the interacting elliptical-holes and cracks to a system of algebraic equations, in which the Fourier-series terms, applied to derive the fundamental solutions, needs to be introduced in order to obtain interacting SIFs of high accuracy, but decreases computation efficiency [24, 25]. To sum up, these methods are difficult to satisfy the requirements of accuracy and efficiency simultaneously in dealing with the problem of multiple elliptical-holes and cracks. Moreover, they are only related to far-field uniform stress without considering surface stress on the elliptical-holes and cracks. Recently, our research group [26] proposed a new integral equation method with simplicity, non-singularity and high accuracy to solve the problem of multiple circular-holes and cracks under both far-field and surface stresses. This new method is promising to be developed for dealing with the problem of multiple elliptical-holes and cracks under the same complex loadings.

In this study, based on Cauchy integral theorem, exact fundamental stress solutions (Section 2.1) of single elliptical-hole under arbitrarily concentrated surface normal and shear forces are derived to establish new integral equations (Section 2.2) for calculating interacting SIFs of multiple elliptical-holes and cracks under both far-field and arbitrary surface stresses, which can be solved by compound trapezoidal and Chebyshev quadrature rules in numerical methods (Sections 2.3 and 2.4). And then, our calculation solutions of interacting SIFs, for one elliptical-hole and one crack (Section 3.1), multiple elliptical-holes and one crack (Section 3.2) and one elliptical-hole and one oriented crack subjected to far-field and nonuniform surface stresses (Section 3.3), are compared with those calculated by Green's function, displacement discontinuity, singular integral equation, pseudo-dislocations and finite element methods, in order to verify validity of this new integral method. Finally, several example solutions are given to further investigate effect of far-field stresses, surface stresses and geometries of elliptical-holes and cracks on interacting SIFs of crack-tips (Section 4).

2 Integral equation method for problem of multiple elliptical-holes and cracks

The two-dimensional in-plane problem involving H elliptical-holes and K straight cracks in an infinite elastic body is plotted in Fig. 1. The applied loadings consist of far-field tensile and shear stresses (σ_{xx}^∞ , σ_{yy}^∞ and $\tau_{xy}^\infty = \tau_{yx}^\infty$) and arbitrary normal and tangential surface stresses on the elliptical-holes (n_h , t_h) and cracks (p_k , q_k), in which tension is dealt

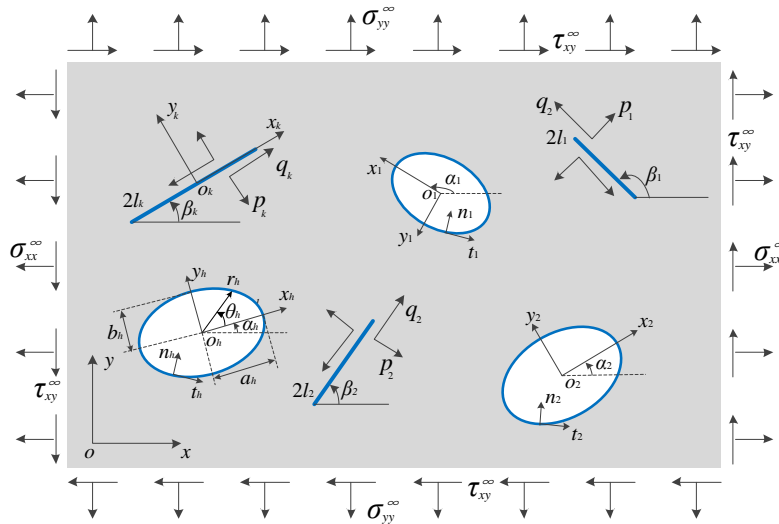


Figure 1: Multiple elliptical-holes and cracks in an infinite elastic body under both far-field and arbitrary surface stresses.

with as the positive. Besides a global Cartesian coordinate system (xoy) , H local Cartesian coordinate systems $(x_h o_h y_h)$ and H local polar coordinate systems $(o_h r_h)$ are set at each elliptical-center o_h ($h = 1, \dots, H$), respectively, where x axis is horizontal and x_h axis is aligned with the major axis of the h -th ellipse. Also, K local Cartesian coordinate systems $(x_k o_k y_k)$ are set at each crack-center ($k = 1, \dots, K$), where x_k axis is aligned with the k -th crack. Let a_h, b_h and α_h represent the major and minor half-lengths of ellipse and its orientation angle with respect to horizontal direction ($a_h \geq b_h, 0 \leq \alpha_h < \pi$), and l_k and β_k represent crack half-length and its orientation angle with respect to horizontal direction ($0 \leq \beta_k < \pi$).

2.1 Exact fundamental stress solutions

For solving the problem involving multiple elliptical-holes and cracks, it is a necessity to obtain normal traction and tangential traction at any point, induced by concentrated surface forces on the elliptical-hole and crack, respectively.

(1) Stresses of single elliptical-hole subjected to concentrated surface forces.

Consider one elliptical-hole (with major and minor half-lengths a, b) in an infinite elastic body subjected to concentrated surface forces (N, T) at arbitrary point A , as plotted in Fig. 2. Two Cartesian coordinate systems are set at the elliptical-center (xoy) and factitious crack-center $(x' o' y')$, respectively, and a polar coordinate systems is set at the elliptical-center (or) . Based on the elasticity theory of Muskhelishvili [27], the normal traction $(\sigma_{y'y'}^e)$ and tangential traction $(\tau_{x'y'}^e)$ at arbitrary point B located on factitious

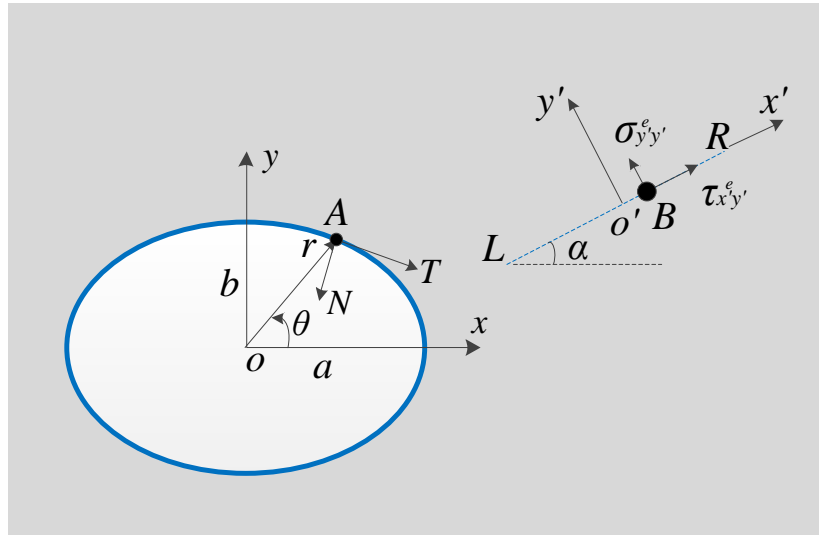


Figure 2: Single elliptical-hole in an infinite elastic body under concentrated surface forces.

crack LR (orientation angle α) are calculated as follows.

Considering the far-field stresses are equal to zero, the following complex functions $\varphi_1(z)$, $\psi_1(z)$ in terms of z can be expressed as:

$$\varphi_1(z) = -\frac{1}{2\pi(1+\kappa)}(f_x + if_y)\ln z + \varphi_0(z), \tag{2.1a}$$

$$\psi_1(z) = \frac{\kappa}{2\pi(1+\kappa)}(f_x - if_y)\ln z + \psi_0(z), \tag{2.1b}$$

in which κ is the parameter of material, related to Poisson's ratio ν , $\kappa = 3 - 4\nu$ under plane stress state, $\kappa = (3 - \nu) / (1 + \nu)$ under plane strain state, f_x and f_y are the principle vectors of concentrated surface forces (N, T) in x - and y - directions, respectively, which can be obtained by:

$$f_x + if_y = -(N + iT)e^{i\gamma}, \tag{2.2a}$$

$$f_x - if_y = -(N - iT)e^{-i\gamma}, \tag{2.2b}$$

in which γ represents the angle between the x axis and the outward normal vector of point A on the boundary of ellipse ($0 \leq \gamma \leq 2\pi$).

According to conformal mapping:

$$z = x + iy = w(\zeta) = R\left(\zeta + \frac{c}{\zeta}\right), \tag{2.3a}$$

$$R = \frac{a+b}{2}, \quad c = \frac{a-b}{a+b}, \tag{2.3b}$$

the ellipse of z -plane can be mapped to the unit circle of ζ -plane.

And thus, it is readily obtained from Eq. (2.1) that

$$\varphi_1(\zeta) = -\frac{1}{2\pi(1+\kappa)}(f_x + if_y)\ln\zeta + \varphi_0(\zeta), \tag{2.4a}$$

$$\psi_1(\zeta) = \frac{\kappa}{2\pi(1+\kappa)}(f_x - if_y)\ln\zeta + \psi_0(\zeta), \tag{2.4b}$$

$$\zeta = \begin{cases} \frac{z + \sqrt{z^2 - 4R^2c}}{2R}, & \text{Re}(z) \geq 0, \\ \frac{z - \sqrt{z^2 - 4R^2c}}{2R}, & \text{Re}(z) < 0, \end{cases} \tag{2.4c}$$

in which $\varphi_1(\zeta)$ and $\psi_1(\zeta)$ are complex functions in the exterior regions of unit-circle, and they need meet the following boundary conditions of the unit circle contour:

$$f(\sigma) = i \int (f_x + if_y)ds = -i \int (N + iT)e^{i\gamma}ds, \tag{2.5a}$$

$$\bar{f}(\bar{\sigma}) = -i \int (f_x - if_y)ds = i \int (N - iT)e^{-i\gamma}ds. \tag{2.5b}$$

Based on the Cauchy integral theorem, there are

$$\varphi_0(\zeta) = -\frac{1}{2\pi i} \int_{\gamma} \left[\frac{f(\sigma)}{\sigma - \zeta} + \frac{(f_x + if_y)\ln\sigma}{2\pi(\sigma - \zeta)} + \frac{(f_x - if_y)}{2\pi(1+\kappa)(\sigma - \zeta)} \frac{\sigma^2 + c}{1 - c\sigma^2} \right] d\sigma, \tag{2.6a}$$

$$\begin{aligned} \psi_0(\zeta) = & -\frac{1}{2\pi i} \int_{\gamma} \left[\frac{\bar{f}(\bar{\sigma})}{\sigma - \zeta} - \frac{(f_x - if_y)\ln\sigma}{2\pi(\sigma - \zeta)} + \frac{(f_x + if_y)}{2\pi(1+\kappa)(\sigma - \zeta)} \frac{1 + c\sigma^2}{\sigma^2 - c} \right] d\sigma \\ & - \zeta \frac{1 + c\zeta^2}{\zeta^2 - c} \varphi_0'(\zeta), \end{aligned} \tag{2.6b}$$

in which the overbar denotes the conjugate of complex number.

Solving Eq. (2.6) and considering $\zeta = w^{-1}(z)$ result in the expressions:

$$\varphi_1(z) = \frac{(N + iT)e^{i\gamma}}{2\pi} \left[\ln(\sigma_1 - \zeta) - \frac{\kappa}{1 + \kappa} \ln\zeta \right], \tag{2.7a}$$

$$\begin{aligned} \psi_1(z) = & \frac{-(N - iT)e^{-i\gamma}}{2\pi} \left[\ln(\sigma_1 - \zeta) - \frac{\ln\zeta}{1 + \kappa} \right] \\ & - \frac{(N + iT)e^{i\gamma}}{2\pi} \left[\frac{1}{1 + \kappa} \frac{1 + c^2}{\zeta^2 - c} - \frac{1 + c\zeta^2}{\zeta^2 - c} \left(1 + \frac{\zeta}{\sigma_1 - \zeta} \right) \right], \end{aligned} \tag{2.7b}$$

in which point σ_1 is located on the unit circle of ζ -plane, corresponding to point z_1 located on ellipse of z -plane.

Application of coordinate transformations [27] leads to the following normal tractions ($\sigma_{y'y'}^e$) and tangential tractions ($\tau_{x'y'}^e$) at arbitrary point B on factitious crack LR , caused by the concentrated surface forces on the elliptical-hole

$$\sigma_{y'y'}^e + i\tau_{x'y'}^e = \varphi_1'(z) + \bar{\varphi}_1'(\bar{z}) + e^{2i\alpha} [\bar{z}\varphi_1''(z) + \psi_1'(z)]. \tag{2.8}$$

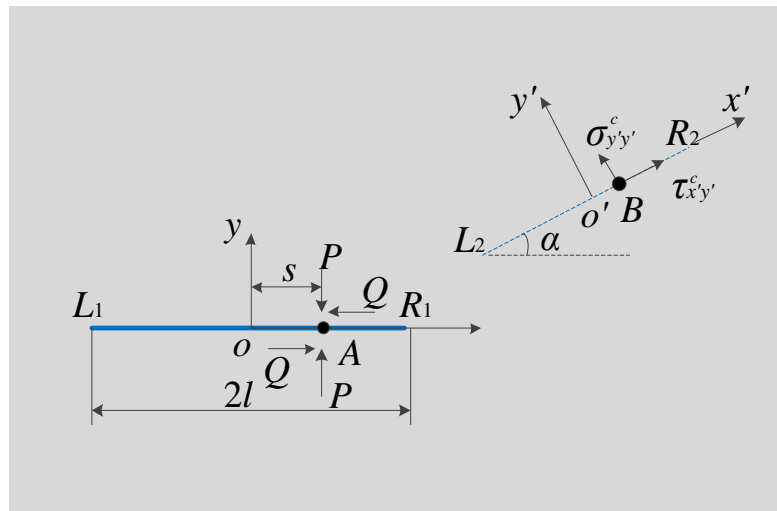


Figure 3: Single crack in an infinite elastic body under concentrated surface forces.

Note here that the derived fundamental stress solutions are powerfully analytical and exact. They have the simpler formulation and higher calculation efficiency than those solved by Fourier series method [27]. That is because Fourier series method is to adopt series to approximate the boundary conditions infinitely and larger series terms (for obtaining stress solution with higher-accuracy) leads to decrease of calculation efficiency.

(2) Stresses of single crack subjected to concentrated surface forces.

Fig. 3 plots one horizontal crack (half-length l) in an infinite elastic body subjected to two pairs of concentrated surface forces (P, Q) at arbitrary point $A(s, 0)$. Two Cartesian coordinate systems $(xoy, x'o'y')$ are set at the centers of the crack L_1R_1 and fictitious crack L_2R_2 (orientation angle α), respectively.

The normal tractions $(\sigma_{y'y'}^c)$ and tangential tractions $(\tau_{x'y'}^c)$ at arbitrary point B located on fictitious crack L_2R_2 , induced by concentrated surface forces (P, Q) , can be given by [26, 28]

$$\begin{aligned} \sigma_{y'y'}^c - i\tau_{x'y'}^c = & -\frac{P-iQ}{2\pi i} \sqrt{s^2-l^2} [G(z) + e^{-2i\alpha} \overline{G(z)}] \\ & -\frac{P+iQ}{2\pi i} \sqrt{s^2-l^2} [\overline{G(z)}(1-e^{-2i\alpha}) + e^{-2i\alpha}(z-\bar{z})\overline{G'(z)}], \end{aligned} \quad (2.9)$$

in which

$$G(z) = \frac{1}{\sqrt{z^2-l^2}(z-s)}, \quad G'(z) = \frac{l^2+sz-2z^2}{(z^2-l^2)^{3/2}(z-s)^2}. \quad (2.10)$$

2.2 Integral equations for determining interacting surface tractions

Consider H elliptical-holes and K straight cracks in an infinite elastic body, subjected to far-field stresses ($\sigma_{xx}^\infty, \sigma_{yy}^\infty$ and τ_{xy}^∞) and arbitrary surface stresses on the elliptical-holes ($n_b(\theta_h), t_l(\theta_b)$) and ($p_k(s_k), q_k(s_k)$) as presented in Fig. 1. The interacting surface tractions on the elliptical-holes and cracks can be solved as follows.

From the obtained fundamental stress solutions (Eqs. (2.7)-(2.8) and Eqs. (2.9)-(2.10)), the new integral equations for the h -th elliptical-hole can be expressed as [26]:

$$\begin{aligned}
 & n_h^\infty(\theta_h) + n_h(\theta_h) \\
 &= N_h(\theta_h) + \sum_{m=1, m \neq h}^H \int_0^{C_m} [N_m(\theta_m)G_{nn,mh}(\theta_m, \theta_h) + T_m(\theta_m)G_{tn,mh}(\theta_m, \theta_h)]dc_m(\theta_m) \\
 & \quad + \sum_{r=1}^K \int_{-l_r}^{l_r} [P_r(s_r)F_{nn,rh}(s_r, \theta_h) + Q_r(s_r)F_{tn,rh}(s_r, \theta_h)]ds_r, \quad 0 < \theta_h < 2\pi, \quad h=1, \dots, H, \quad (2.11a)
 \end{aligned}$$

$$\begin{aligned}
 & t_h^\infty(\theta_h) + t_h(\theta_h) \\
 &= T_h(\theta_h) + \sum_{m=1, m \neq h}^H \int_0^{C_m} [N_m(\theta_m)G_{nt,mh}(\theta_m, \theta_h) + T_m(\theta_m)G_{tt,mh}(\theta_m, \theta_h)]dc_m(\theta_m) \\
 & \quad + \sum_{r=1}^K \int_{-l_r}^{l_r} [P_r(s_r)F_{nt,rh}(s_r, \theta_h) + Q_r(s_r)F_{tt,rh}(s_r, \theta_h)]ds_r, \quad 0 < \theta_h < 2\pi, \quad h=1, \dots, H, \quad (2.11b)
 \end{aligned}$$

in which $n_h^\infty(\theta_h)$ and $t_h^\infty(\theta_h)$ are the normal and tangential surface tractions on the h -th elliptical-hole, attributed to remote stresses, respectively, which has the same magnitude and opposite direction as the far-field stresses

$$n_h^\infty(\theta_h) = -\sigma_{xx}^\infty \cos^2(\alpha_h + \gamma_h) - \sigma_{yy}^\infty \sin^2(\alpha_h + \gamma_h) + \tau_{xy}^\infty \sin 2(\alpha_h + \gamma_h), \quad (2.12a)$$

$$t_h^\infty(\theta_h) = (\sigma_{yy}^\infty - \sigma_{xx}^\infty) \sin(\alpha_h + \gamma_h) \cos(\alpha_h + \gamma_h) - \tau_{xy}^\infty \cos 2(\alpha_h + \gamma_h), \quad (2.12b)$$

in which α_h is the orientation angle of the h -th elliptical-hole, and γ_h represents the angle between the x_h axis and the outward normal vector of point (r_h, θ_h) on the boundary of the h -th elliptical-hole ($0 \leq \gamma_h \leq 2\pi$).

Similarly, the integral equations for the k -th crack can be expressed as:

$$\begin{aligned}
 & p_k^\infty(s_k) + p_k(s_k) \\
 &= P_k(s_k) + \sum_{m=1}^H \int_0^{C_m} [N_m(\theta_m)G_{nn,mk}(\theta_m, s_k) + T_m(\theta_m)G_{tn,mk}(\theta_m, s_k)]dc_m(\theta_m)
 \end{aligned}$$

$$\begin{aligned}
 & + \sum_{r=1, r \neq k}^K \int_{-l_r}^{l_r} [P_r(s_r)F_{nn,rk}(s_r, s_k) + Q_r(s_r)F_{tn,rk}(s_r, s_k)] ds_r, \quad -l_k < s_k < l_k, \quad k=1, \dots, K, \quad (2.13a) \\
 & q_k^\infty(s_k) + q_k(s_k) \\
 & = Q_k(s_k) + \sum_{m=1}^H \int_0^{C_m} [N_m(\theta_m)G_{nt,mk}(\theta_m, s_k) + T_m(\theta_m)G_{tt,mk}(\theta_m, s_k)] dc_m(\theta_m) \\
 & + \sum_{r=1, r \neq k}^K \int_{-l_r}^{l_r} [P_r(s_r)F_{nt,rk}(s_r, s_k) + Q_r(s_r)F_{tt,rk}(s_r, s_k)] ds_r, \quad -l_k < s_k < l_k, \quad k=1, \dots, K, \quad (2.13b)
 \end{aligned}$$

in which $p_k^\infty(\theta_k)$ and $q_k^\infty(\theta_k)$ are the known normal and tangential surface tractions on the k -th crack, attributed to the far-field stresses, respectively, which can be given by:

$$p_k^\infty(s_k) = -\sigma_{xx}^\infty \sin^2 \beta_k - \sigma_{yy}^\infty \cos^2 \beta_k + \tau_{xy}^\infty \sin 2\beta_k, \quad (2.14a)$$

$$q_k^\infty(s_k) = (\sigma_y^\infty - \sigma_{xx}^\infty) \sin \beta_k \cos \beta_k - \tau_{xy}^\infty \cos 2\beta_k, \quad (2.14b)$$

in which β_k is the orientation angle of k -th crack.

In Eqs. (2.11) and (2.13), $N_h(\theta_h)$, $T_h(\theta_h)$ stand for the interacting normal and tangential tractions to be determined on the surface of the h -th elliptical-hole, respectively. $P_k(s_k)$, $Q_k(s_k)$ stand for the interacting normal and tangential tractions to be determined on the surface of the k -th crack, respectively. $c_m(\theta_m)$ stands for the arc-length of the m -th elliptical-hole, which is related to θ_m , and C_m stands for the perimeter of the m -th elliptical-hole. The kernel functions G and F have a definitely physical meaning, for instance, $G_{nn,mk}(\theta_m, s_k)$ and $G_{nt,mk}(\theta_m, s_k)$ mean the normal and tangential surface tractions of arbitrary point $(s_k, 0)$ on the k -th crack, caused by unit concentrated normal force of arbitrary point $z_m(r_m, \theta_m)$ on the m -th elliptical-hole, respectively. They can be obtained by substitution of $N=1$ and $T=0$ into the first fundamental stress solutions in Eqs. (2.7)-(2.8) as:

$$G_{nm,mk}(\theta_m, s_k) + iG_{nt,mk}(\theta_m, s_k) = \varphi_1'(z_k) + \bar{\varphi}_1'(\bar{z}_k) + e^{2i\beta_k} [\bar{z}_k \varphi_1''(z_k) + \psi_1'(z_k)] \quad (2.15)$$

and

$$\varphi_1(z_k) = \frac{e^{i\gamma_m}}{2\pi} \left[\ln(\sigma_{1m} - \zeta_k) - \frac{\kappa}{1+\kappa} \ln \zeta_k \right], \quad (2.16a)$$

$$\begin{aligned}
 \psi_1(z_k) = & \frac{-e^{-i\gamma_m}}{2\pi} \left[\ln(\sigma_{1m} - \zeta_k) - \frac{\ln \zeta_k}{1+\kappa} \right] \\
 & - \frac{e^{i\gamma_m}}{2\pi} \left[\frac{1}{1+\kappa} \frac{1+c_m^2}{\zeta_k^2 - c_m} - \frac{1+c_m \zeta_k^2}{\zeta_k^2 - c_m} \left(1 + \frac{\zeta_k}{\sigma_{1m} - \zeta_k} \right) \right], \quad (2.16b)
 \end{aligned}$$

and $G_{tn,mh}(\theta_m, \theta_h)$ and $G_{tt,mh}(\theta_m, \theta_h)$ mean the normal and tangential surface tractions of arbitrary point $z_h(r_h, \theta_h)$ on the h -th elliptical-hole, caused by unit concentrated tangential force of arbitrary point $z_m(r_m, \theta_m)$ on the m -th elliptical-hole, respectively. They can be

obtained by substitution of $N=0$ and $T=1$ into the first fundamental stress solutions in Eqs. (2.7)-(2.8) as:

$$G_{tn,mh}(\theta_m, \theta_h) + iG_{tt,mh}(\theta_m, \theta_h) = \varphi_1'(z_h) + \bar{\varphi}_1'(\bar{z}_h) - e^{2i(\alpha_h + \gamma_h)} [\bar{z}_h \varphi_1''(z_h) + \psi_1'(z_h)] \quad (2.17)$$

and

$$\varphi_1(z_h) = \frac{ie^{i\gamma_m}}{2\pi} \left[\ln(\sigma_{1m} - \zeta_h) - \frac{\kappa}{1+\kappa} \ln \zeta_h \right], \quad (2.18a)$$

$$\begin{aligned} \psi_1(z_h) = & \frac{ie^{-i\gamma_m}}{2\pi} \left[\ln(\sigma_{1m} - \zeta_h) - \frac{\ln \zeta_h}{1+\kappa} \right] \\ & - \frac{ie^{i\gamma_m}}{2\pi} \left[\frac{1}{1+\kappa} \frac{1+c_m^2}{\zeta_h^2 - c_m} - \frac{1+c_m\zeta_h^2}{\zeta_h^2 - c_m} \left(1 + \frac{\zeta_h}{\sigma_{1m} - \zeta_h} \right) \right]. \end{aligned} \quad (2.18b)$$

Similarly, the kernel functions $F_{nn,rh}(s_r, \theta_h)$ and $F_{nt,rh}(s_r, \theta_h)$ mean the normal and tangential surface tractions of arbitrary point $z_h(r_h, \theta_h)$ on the h -th elliptical-hole, caused by unit concentrated normal force of arbitrary point $(s_r, 0)$ on the r -th crack, respectively, which can be determined by taking $P=1$ and $Q=0$ in the second fundamental stress solutions from Eqs. (2.9)-(2.10)

$$\begin{aligned} & F_{nn,rh}(s_r, \theta_h) + iF_{nt,rh}(s_r, \theta_h) \\ & = -\frac{1}{2\pi i} \sqrt{s_r^2 - l_r^2} [G(z_h) - e^{-2i(\alpha_h + \gamma_h)} \overline{G(z_h)}] \\ & \quad - \frac{1}{2\pi i} \sqrt{s_r^2 - l_r^2} [\overline{G(z_h)}(1 + e^{-2i(\alpha_h + \gamma_h)}) - e^{-2i(\alpha_h + \gamma_h)} (z_h - \bar{z}_h) \overline{G'(z_h)}], \end{aligned} \quad (2.19a)$$

$$G(z_h) = \frac{1}{\sqrt{z_h^2 - l_r^2} (z_h - s_r)}, \quad G'(z_h) = \frac{l_r^2 + s_r z_h - 2z_h^2}{(z_h^2 - l_r^2)^{3/2} (z_h - s_r)^2} \quad (2.19b)$$

and $F_{tn,rk}(s_r, s_k)$ and $F_{tt,rk}(s_r, s_k)$ mean the normal and tangential surface tractions of arbitrary point $(s_k, 0)$ on the k -th crack, caused by unit concentrated normal force of arbitrary point $(s_r, 0)$ on the r -th crack, respectively, which can be determined by taking $P=0$ and $Q=1$ in the second fundamental stress solutions from Eqs. (2.9)-(2.10)

$$\begin{aligned} & F_{tn,rk}(s_r, s_k) + iF_{tt,rk}(s_r, s_k) \\ & = \frac{i}{2\pi i} \sqrt{s_r^2 - l_r^2} [G(z_k) + e^{-2i\beta_k} \overline{G(z_k)}] \\ & \quad - \frac{i}{2\pi i} \sqrt{s_r^2 - l_r^2} [\overline{G(z_k)}(1 - e^{-2i\beta_k}) + e^{-2i\beta_k} (z_k - \bar{z}_k) \overline{G'(z_k)}], \end{aligned} \quad (2.20a)$$

$$G(z_k) = \frac{1}{\sqrt{z_k^2 - l_r^2} (z_k - s_r)}, \quad G'(z_k) = \frac{l_r^2 + s_r z_k - 2z_k^2}{(z_k^2 - l_r^2)^{3/2} (z_k - s_r)^2} \quad (2.20b)$$

2.3 Numerical solution of integral equations

Based on compound trapezoidal rule and Chebyshev quadrature rule [29], these integral equations (2.11) and (2.13) are readily expressed as the following linear algebraic equations:

$$\begin{aligned}
 & n_h^\infty(\theta_h^i) + n_h(\theta_h^i) \\
 &= N_h(\theta_h^i) + \sum_{m=1, m \neq h}^H \sum_{j=1}^M [N_m(\theta_m^j) G_{nn, mh}(\theta_m^j, \theta_h^i) + T_m(\theta_m^j) G_{tn, mh}(\theta_m^j, \theta_h^i)] \omega_m(\theta_m^j) \\
 &+ \sum_{r=1}^K \sum_{j=1}^M [P_r(s_r^j) F_{nn, rh}(s_r^j, \theta_h^i) + Q_r(s_r^j) F_{tn, rh}(s_r^j, \theta_h^i)] \delta_r^j, \quad (i, j = 1, \dots, M), \tag{2.21a}
 \end{aligned}$$

$$\begin{aligned}
 & t_h^\infty(\theta_h^i) + t_h(\theta_h^i) \\
 &= T_h(\theta_h^i) + \sum_{m=1, m \neq h}^H \sum_{j=1}^M [N_m(\theta_m^j) G_{nt, mh}(\theta_m^j, \theta_h^i) + T_m(\theta_m^j) G_{tt, mh}(\theta_m^j, \theta_h^i)] \omega_m(\theta_m^j) \\
 &+ \sum_{r=1}^K \sum_{j=1}^M [P_r(s_r^j) F_{nt, rh}(s_r^j, \theta_h^i) + Q_r(s_r^j) F_{tt, rh}(s_r^j, \theta_h^i)] \delta_r^j, \quad (i, j = 1, \dots, M), \tag{2.21b}
 \end{aligned}$$

and

$$\begin{aligned}
 & p_k^\infty(s_k^i) + p_k(s_k^i) \\
 &= P_k(s_k^i) + \sum_{m=1}^H \sum_{j=1}^M [N_m(\theta_m^j) G_{nn, mk}(\theta_m^j, s_k^i) + T_m(\theta_m^j) G_{tn, mk}(\theta_m^j, s_k^i)] \omega_m(\theta_m^j) \\
 &+ \sum_{r=1, r \neq k}^K \sum_{j=1}^M [P_r(s_r^j) F_{nn, rk}(s_r^j, s_k^i) + Q_r(s_r^j) F_{tn, rk}(s_r^j, s_k^i)] \delta_r^j, \quad (i, j = 1, \dots, M), \tag{2.22a}
 \end{aligned}$$

$$\begin{aligned}
 & q_k^\infty(s_k^i) + q_k(s_k^i) \\
 &= Q_k(s_k^i) + \sum_{m=1}^H \sum_{j=1}^M [N_m(\theta_m^j) G_{nt, mk}(\theta_m^j, s_k^i) + T_m(\theta_m^j) G_{tt, mk}(\theta_m^j, s_k^i)] \omega_m(\theta_m^j) \\
 &+ \sum_{r=1, r \neq k}^K \sum_{j=1}^M [P_r(s_r^j) F_{nt, rk}(s_r^j, s_k^i) + Q_r(s_r^j) F_{tt, rk}(s_r^j, s_k^i)] \delta_r^j, \quad (i, j = 1, \dots, M), \tag{2.22b}
 \end{aligned}$$

with

$$s_k^i = l_k \cos \frac{(2i-1)\pi}{2M}, \quad s_r^j = l_r \cos \frac{(2j-1)\pi}{2M}, \tag{2.23a}$$

$$\theta_h^i = \frac{(i-1)2\pi}{M}, \quad \theta_m^j = \frac{(j-1)2\pi}{M}, \quad i, j = 1, \dots, M, \tag{2.23b}$$

in which M is the number of line segments or nodes on the boundaries of elliptical-holes and cracks; $N_h(\theta_h^i)$, $T_h(\theta_h^i)$ are interacting normal and tangential surface tractions

to be determined on the i -th arc of the h -th elliptical-hole, respectively. $P_h(s_k^i)$, $Q_b(s_h^i)$ are interacting normal and tangential surface tractions to be determined on the i -th line segment of the k -th crack, respectively. $\omega_\infty(\theta_m^j)$ and δ_r^j represent the j -th arc length of the m -th elliptical-hole and the j -th line segment length of the r -th crack, respectively, which are given by:

$$\omega_m(\theta_m^j) = \int_{\varphi_m^{j-1}}^{\varphi_m^j} \sqrt{a_m^2 \sin^2 \varphi_m + b_m^2 \cos^2 \varphi_m} d\varphi_m, \tag{2.24a}$$

$$\delta_r^j = \frac{\pi l_r}{M} \sin \frac{(2j-1)\pi}{2M}, \quad j=1, \dots, M, \tag{2.24b}$$

and

$$\varphi_m^j = \begin{cases} \arctan \left[\frac{a_m}{b_m} \tan \frac{(2j-1)\pi}{M} \right], & -\frac{\pi}{2} \leq \frac{(2j-1)\pi}{M} \leq \frac{\pi}{2}, \\ \pi + \arctan \left[\frac{a_m}{b_m} \tan \frac{(2j-1)\pi}{M} \right], & \frac{\pi}{2} < \frac{(2j-1)\pi}{M} \leq \frac{3\pi}{2}, \\ 2\pi + \arctan \left[\frac{a_m}{b_m} \tan \frac{(2j-1)\pi}{M} \right], & \frac{3\pi}{2} < \frac{(2j-1)\pi}{M} < 2\pi. \end{cases} \tag{2.25}$$

These linear algebraic equations in Eqs. (2.21)-(2.22) can be written as the form of matrix:

$$AX = \begin{bmatrix} A_{11} & \cdots & A_{1H} & \cdots & A_{1(H+K)} \\ \cdots & \cdots & \cdots & \cdots & \cdots \\ A_{H1} & \cdots & A_{HH} & \cdots & A_{H(H+K)} \\ \cdots & \cdots & \cdots & \cdots & \cdots \\ A_{(H+K)1} & \cdots & A_{(H+K)L} & \cdots & A_{(H+K)(H+K)} \end{bmatrix} \begin{bmatrix} X_1 \\ \cdots \\ X_H \\ \cdots \\ X_{(H+K)} \end{bmatrix} = \begin{bmatrix} B_1 \\ \cdots \\ B_H \\ \cdots \\ B_{(H+K)} \end{bmatrix} = B, \tag{2.26}$$

in which where submatrix A_{ij} consists of $2M \times 2M$ elements; when $i=j$, A_{ij} stands for an unit submatrix related to the elliptical-hole or crack itself; when $i \neq j$, A_{ij} stands for influence of a certain elliptical-hole on the other elliptical-holes (or cracks), or a certain crack on the elliptical-holes (or the other cracks). X_j stands for a submatrix to be undetermined, which means the interacting surface tractions on the elliptical-holes and cracks. B_j is a known submatrix related to far-field stresses and surface stresses on the elliptical-holes and cracks. Obviously, the undetermined submatrix X_j can be determined uniquely by Eq. (2.26).

2.4 Interacting stress intensity factors

In order to calculate the interacting SIFs, it is necessary to obtain the SIFs of single crack under concentrated surface forces.

When one crack L_1R_1 (half-length l) in an infinite elastic body is subjected to concentrated surface forces (P, Q) at point $A(s,0)$, (see Fig. 3), The SIFs K_I and K_{II} can be written

by [30]:

$$K_I(\pm) = \frac{P}{\sqrt{\pi l}} \sqrt{\frac{l \pm s}{l \mp s}}, \quad K_{II}(\pm) = \frac{Q}{\sqrt{\pi l}} \sqrt{\frac{l \pm s}{l \mp s}}, \quad (2.27)$$

in which the lower and upper superscripts stand for the right and left tips of the crack, respectively.

From Eq. (2.27), the interacting SIFs of the k -th crack are written by $P_k(s_k)$, $Q_k(s_k)$ from the integral equations in Eqs. (2.11) and (2.13) as follows:

$$K_{I,k}^\pm = \frac{1}{\sqrt{\pi l_k}} \int_{-l_k}^{l_k} P_k(s_k) \sqrt{\frac{l_k \pm s_k}{l_k \mp s_k}} ds_k, \quad (2.28a)$$

$$K_{II,k}^\pm = \frac{1}{\sqrt{\pi l_k}} \int_{-l_k}^{l_k} Q_k(s_k) \sqrt{\frac{l_k \pm s_k}{l_k \mp s_k}} ds_k. \quad (2.28b)$$

Based on the Chebyshev quadrature rule [27]:

$$\int_{-l}^l \frac{f(x)}{\sqrt{l^2 - x^2}} dx = \frac{\pi}{M} \sum_{i=1}^M f(x^i), \quad x^i = l \cos \frac{(2i-1)\pi}{2M}, \quad (2.29)$$

the interacting SIFs K_I and K_{II} of the right and left crack-tips can be given, respectively, by:

$$K_{I,k}^\pm = \frac{\sqrt{\pi l_k}}{M} \sum_{i=1}^M P_k(s_k^i) \left(1 \pm \frac{s_k^i}{l_k}\right), \quad (2.30a)$$

$$K_{II,k}^\pm = \frac{\sqrt{\pi l_k}}{M} \sum_{i=1}^M Q_k(s_k^i) \left(1 \pm \frac{s_k^i}{l_k}\right), \quad s_k^i = l_k \cos \frac{(2i-1)\pi}{2M}, \quad (2.30b)$$

in which the interacting normal and tangential surface tractions $P_h(s_k^i)$, $Q_b(s_k^i)$ can be calculated from Eq. (2.26).

Note that the integral equation method can also be reduced to solve the problem of multiple cracks or multiple circular-holes and cracks under complex loadings. Also, these integral equations in Eqs. (2.11) and (2.13) are regular without any singular parts and can be easily computed by combination of compound trapezoidal rule and Chebyshev quadrature rule, since the two fundamental stress solutions in Eqs. (2.7)-(2.10) have considered boundary conditions of single circular-hole and single crack. Based on theoretical viewpoints, the accuracy of interacting SIFs depends on the number of nodes M in compound trapezoidal rule and Chebyshev quadrature rule but not this method. The solutions within high accuracy can be obtained only by a larger number of M , since the two fundamental stress solutions are powerfully analytical and exact without any approximations.

3 Verification of the integral equation method

3.1 One elliptical-hole and one crack subjected to far-field tensile or shear stress

In order to illustrate the accuracy of the integral equation method, the interacting SIFs obtained by existing method (e.g., Green’s function, displacement discontinuity and singular integral equation methods) are given for one circular/elliptical-hole and one crack subjected to far-field tensile stress or shear stress.

Fig. 4 depicts a horizontal elliptical-hole (major half-length a , and minor half-length b) and a horizontal crack LR (half-length l) in an infinite elastic body under far-field tensile (σ_{yy}^∞) (only in y -direction) and shear (τ_{xy}^∞) stresses, in which t stands for the distance between the elliptical-center o and the crack-center O in horizontal direction. Using Green’s function method (with singularity), Erdogan et al. [11] obtained the interacting SIFs for the problem of a circular-hole ($a = b$) and a crack ($l = 0.5a$) only under far-field tensile stresses σ_{yy}^∞ ($\tau_{xy}^\infty = 0$), and their calculation results are usually regarded as an exact solutions because of their method’s analyticity [12, 15, 21]. Due to symmetry of loadings and geometries, interacting SIFs of Mode II are always equal to zero (i.e., $K_{II} = 0$). Table 1 only shows the normalized interacting SIFs F_{IL} , F_{IR} ($F_I = K_I / \sigma_{yy}^\infty \sqrt{\pi l}$) of crack-tips L and R , under various distances t/a ($t/a = 3.2, 3.5, 4, 5, 6, 8$) and the number of nodes M ($M = 32, 64, 96, 128$), calculated by our method and Green’s function method ($\nu = 0.25$). It is found that with the increase of t/a , the F_{IL} and F_{IR} values are close to the case of single crack, indicating the influence of the circular hole on the crack becomes smaller and smaller. It can be observed that the larger the M , the closer to Erdogan’s results our results are. When $M \geq 96$, our results are in complete agreement with Erdogan’s results. Therefore, numerical computation are carried out under the condition of $M = 96$ in the subsequent examples in order to obtain the interacting SIFs within high accuracy.

For further showing the accuracy of our method, the interacting SIFs are calculated and compared with displacement discontinuity method of Yan [21] for one horizontal elliptical-hole $o(a, b)$ and one horizontal crack LR ($a/l = 0.2$) only under far-field tensile

Table 1: Comparison of normalized SIFs F_{IL} , F_{IR} between our method and Green’s function method ($a = b = 2l$).

t/a	Our method								Green’s function method	
	$M = 32$		$M = 64$		$M = 96$		$M = 128$		F_{IL}	F_{IR}
	F_{IL}	F_{IR}	F_{IL}	F_{IR}	F_{IL}	F_{IR}	F_{IL}	F_{IR}		
3.2	1.437	2.376	1.418	2.289	1.417	2.274	1.417	2.274	1.417	2.274
3.5	1.291	1.726	1.290	1.722	1.290	1.722	1.290	1.722	1.290	1.722
4	1.188	1.394	1.188	1.394	1.188	1.394	1.188	1.394	1.188	1.394
5	1.102	1.174	1.102	1.174	1.102	1.174	1.102	1.174	1.102	1.174
6	1.065	1.099	1.065	1.099	1.065	1.099	1.065	1.099	1.065	1.099
8	1.033	1.045	1.033	1.045	1.033	1.045	1.033	1.045	1.033	1.045

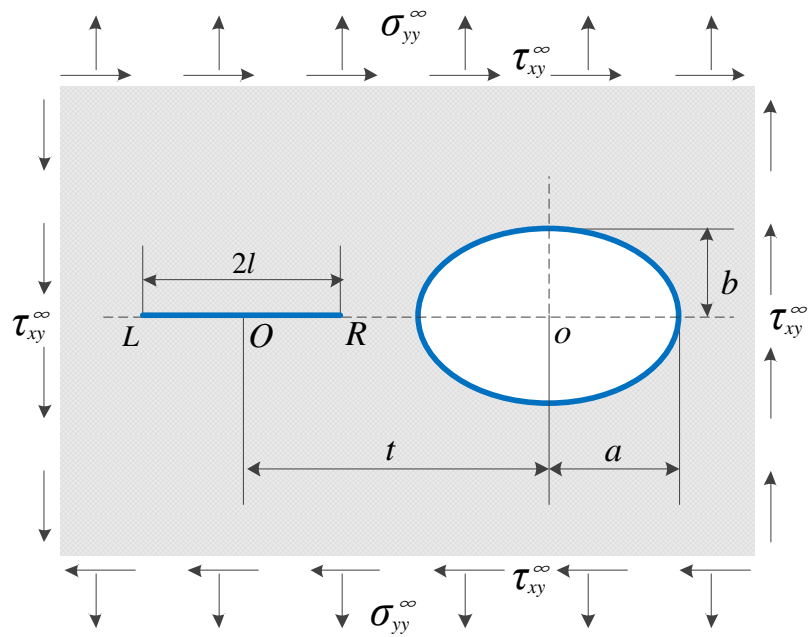


Figure 4: One elliptical-hole and one crack in an infinite elastic body subjected to far-field tensile and shear stresses.

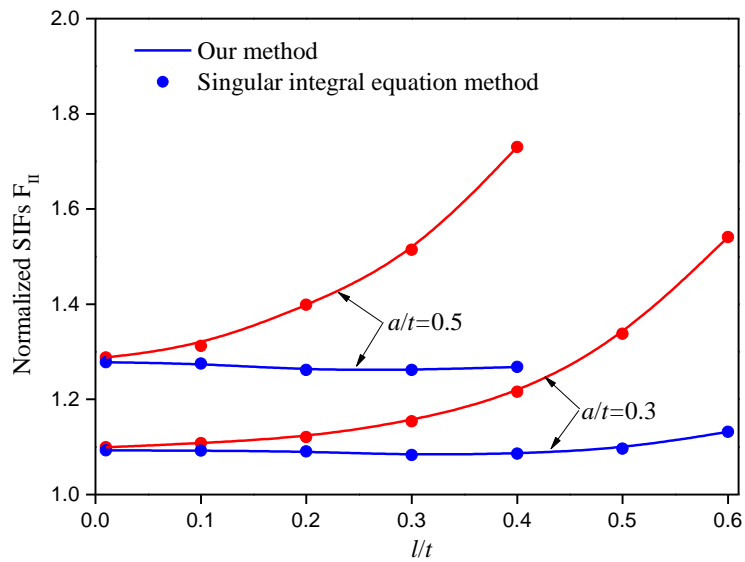


Figure 5: Comparison of normalized SIFs F_{IIL} , F_{IIR} between our method and singular integral equation method.

Table 2: Comparison of normalized SIFs F_{IR} between our method and displacement discontinuity method ($a/l=0.2$).

$a/(t-l)$	Our method			Displacement discontinuity method		
	$b/a=0$	$b/a=0.5$	$b/a=1$	$b/a=0$	$b/a=0.5$	$b/a=1$
0.1	1.0038	1.0044	1.0041	1.0015	1.0022	1.0024
0.2	1.0137	1.0167	1.0163	1.0112	1.0127	1.0146
0.3	1.0299	1.0361	1.0392	1.0270	1.0305	1.0374
0.4	1.0538	1.0666	1.0767	1.0502	1.0580	1.0747
0.5	1.0882	1.1117	1.1343	1.0834	1.0994	1.1318
0.6	1.1383	1.1792	1.2204	1.1311	1.1627	1.2167
0.7	1.2150	1.2838	1.3497	1.2034	1.2657	1.3451
0.8	1.3466	1.4602	1.5540	1.3253	1.4483	1.5447
0.9	1.6420	1.8191	1.9427	1.5908	1.8561	1.9143

stress σ_{yy}^{∞} ($\tau_{xy}^{\infty} = 0$ in Fig. 4). Table 2 presents the normalized SIFs F_{IR} of the internal crack-tip R under various distances $a/(t-l)$ ($a/(t-l) = 0.1 \sim 0.9$) and sizes b/a ($b/a = 0, 0.5, 1$), obtained by our method and the displacement discontinuity method ($\nu=0.3$), in which $b/a=0, 0.5, 1$ stand for horizontal crack, horizontal elliptical-hole and circular-hole, respectively. It can be seen that with the decrease of a/t , the FIR value becomes smaller. As b/a is from 0 (crack) to 0.5 (elliptical-hole) and to 1 (circular-hole), almost all of F_{IR} values are increased for the same $a/(t-l)$, indicating the circular-hole has greater effect on the crack-tip R than elliptical-hole and crack. The comparison manifests that there exists a small differences between our results and Yan's results due to approximation of displacement discontinuity method.

For one horizontal elliptical-hole o ($b/a=0.5$) and one horizontal crack LR ($2l$) only under far-field shear stress τ_{xy}^{∞} ($\tau_{yy}^{\infty} = 0$ in Fig. 4), Tang and Wang [19] give the interacting SIFs of crack-tips L and R by adopting singular integral equation method. Fig. 5 depicts the normalized SIFs F_{IIR}, F_{IIL} ($F_{II} = K_{II}/\tau_{xy}^{\infty}\sqrt{\pi l}$) of crack-tips R and L varying with l/t under various distances a/t ($a/t = 0.3, 0.5$) by our method and singular integral equation method. It is found that present solutions agree very well with Tang and Wang's solutions.

To sum up, these method are either complicated to solve the singular integral equation or difficult to obtain high accurate SIFs. Furthermore, they are only utilized to solve the multiple hole-crack problem under far-field stresses, and the extension to study the case of complex loadings (e.g., nonuniform surface stresses) might encounter difficulty. Comparatively, our method not only can avoid the trouble in calculating the singular integral equations (without any singular parts), but also has high accuracy (due to the exact fundamental solutions) and wider applicability (suitable for both far-field stresses and arbitrarily distributed surface stresses).

3.2 Multiple elliptical-holes and one crack subjected to far-field tensile stress

In order to show the application of the integral equation method, the interacting SIFs obtained by pseudo-dislocations method are considered for multiple elliptical-holes and one crack subjected to far-field tensile stress.

Fig. 6 presents one horizontal crack (l) surrounded by a square array of eight equal elliptical-holes (a, b) under far-field uniaxial tensile stress σ , in which t stands for the distance between two adjacent elliptical-centers or elliptical-center and crack-center in horizontal and vertical directions. Due to symmetry, K_{IL} and K_{IR} have the same values, and K_{IIL} and K_{IIR} are always equal to zero. Fig. 7 only illustrates our solutions of normalized SIFs F_I ($F_I = K_I / \sigma \sqrt{\pi l}$) varying with $l / (t - a)$, as well as the solutions of Han and Wang [23] (pseudo-dislocations method). When two crack-tips are far from elliptical-holes (i.e., the crack length is small), F_I is smaller than 1, which indicates that these elliptical-holes have shielding effect on the crack. When two crack-tips are near to elliptical-holes (i.e., the crack length is large), F_I is larger than 1, which indicates that these elliptical-holes have amplification effect on the crack. It can be observed that the present solutions are in perfect agreement with those in [23].

Compared with pseudo-dislocations method, our method has higher calculation efficiency, since pseudo-dislocations method is to use the Fourier-series to infinitely approx-

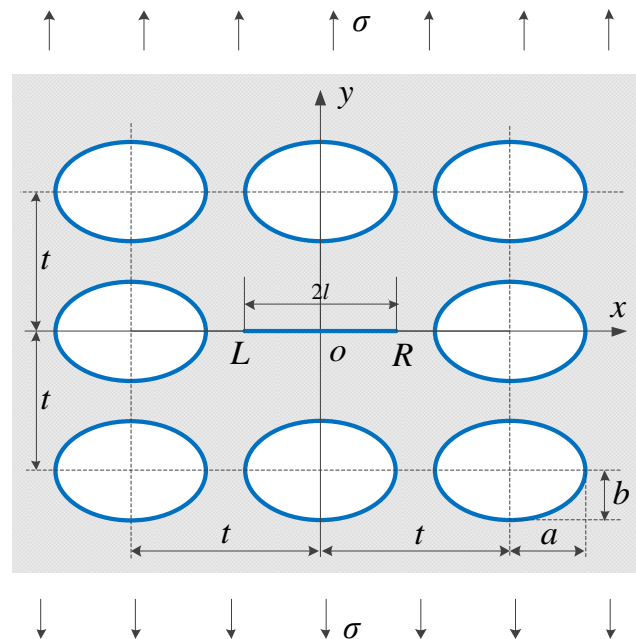


Figure 6: One horizontal crack surrounded by a square array of eight equal elliptical-holes in an infinite elastic body subjected to far-field tensile stress.

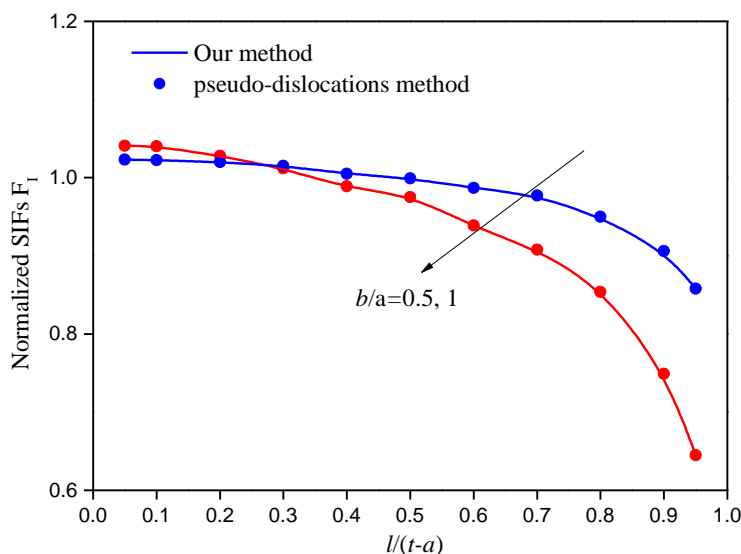


Figure 7: Comparison of normalized SIF F_I between present method and pseudo-dislocations method.

imate the boundary conditions in their fundamental solutions and increasing Fourier-series terms leads to low calculation efficiency [24, 25]. In addition, the method only is available for the multiple hole-crack problem subjected to far-field stresses.

3.3 One elliptical-hole and one oriented crack subjected to far-field tensile and nonuniform surface stress

At present, very few studies are related to the problem of multiple elliptical-holes and cracks under far-field and nonuniform distributed surface stresses. For further showing the effectiveness of the integral equation method, numerical method (by ANSYS software) is applied to determine the interacting SIFs of elliptical-hole and crack under complicated stresses.

Consider an infinite elastic plane with a horizontal elliptical-hole ($a=1.5b=\lambda$) and an oriented crack ($l=1, \beta=45^\circ$) under far-field biaxial tension ($\sigma_{xx}^\infty=0.5\text{MPa}, \sigma_{yy}^\infty=1\text{MPa}$) and surface stress on the elliptical-hole ($n = -\cos^2\theta\text{MPa}$), as presented in Fig. 8, in which t is the distance between the elliptical-center o and the crack-center O in horizontal direction ($t=2$). In order to solve the plane problem of elliptical-hole and crack, the model size is $50\text{m} \times 50\text{m}$ and the type of element is PLANE183. The interacting SIFs K_{IL}, K_{IR}, K_{IIL} and K_{IIR} at crack-tips L and R can be extracted by the interaction integral method after solving stresses and strains at the vicinity of crack-tips. Fig. 9 shows the interacting SIFs K_{IL}, K_{IR}, K_{IIL} and K_{IIR} varying with λ , calculated by our method and ANSYS software. It can be seen that our solutions basically coincide with finite element solutions.

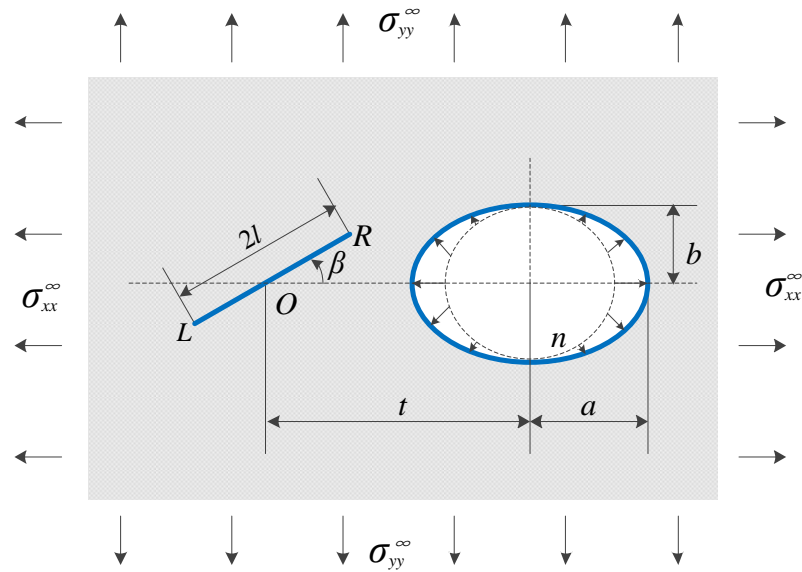


Figure 8: One horizontal elliptical-hole and one oriented crack in an infinite elastic body subjected to far-field tensile stress and surface stress on the elliptical-hole.

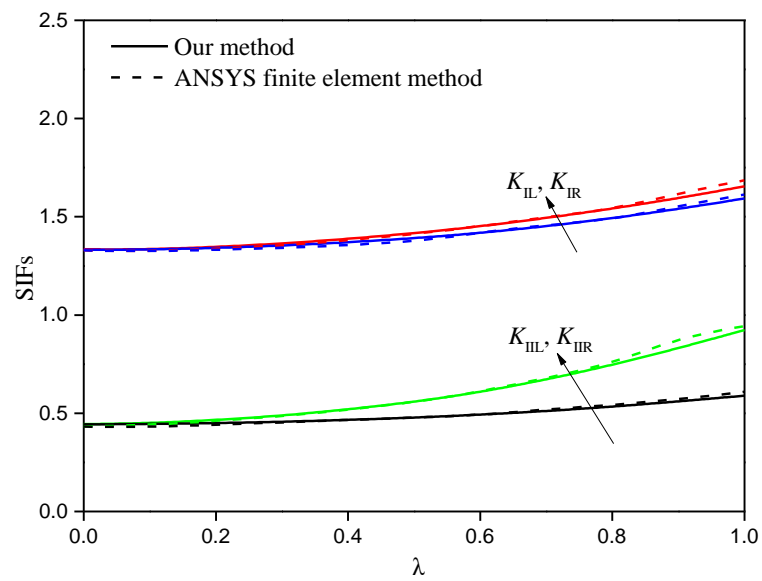


Figure 9: Comparison of interacting SIFs K_{IL} , K_{IR} , K_{IIL} , K_{IIR} between our method and ANSYS finite element method.

Since the finite element method is to utilize shape function interpolation and Gaussian quadrature to denote the unknown field-variables in the whole region and the description of the function interpolation is independent of the mesh refinement, it is suitable for the multiply connected domain problem under complex loadings [31–34]. However, its computation accuracy depends on not only the mesh refinement but also extraction method of SIFs (e.g., contour integral method, displacement correlation method etc.) [35]. Moreover, mesh refinement in the whole region leads to low calculation efficiency.

4 Computational examples

Currently, there are very few literatures on the systematic study of interacting SIFs for the problem of elliptical-hole and crack under far-field and surface stresses. In this section, in order to further investigate influence of elliptical-hole on interacting SIFs, take one elliptical-hole o (major half-length a , and minor half-length b) and one crack LR (half-length l) in an infinite elastic body subjected to various far-field ($\sigma_{xx}^\infty, \sigma_{yy}^\infty$) and surface normal stresses on the elliptical-hole (n) and the crack (p) as a computational example (Fig. 10), in which tension is treated as the positive. The orientation angle of the major axis of ellipse and crack orientation angle are denoted by α, β , respectively, and Poisson’s ratio $\nu = 0.25$. The connecting line of center-to-center between elliptical-hole and crack is horizontal and its distance is denoted by t . The interacting SIFs K_{IL}, K_{IR}, K_{IIL} and K_{IIR}

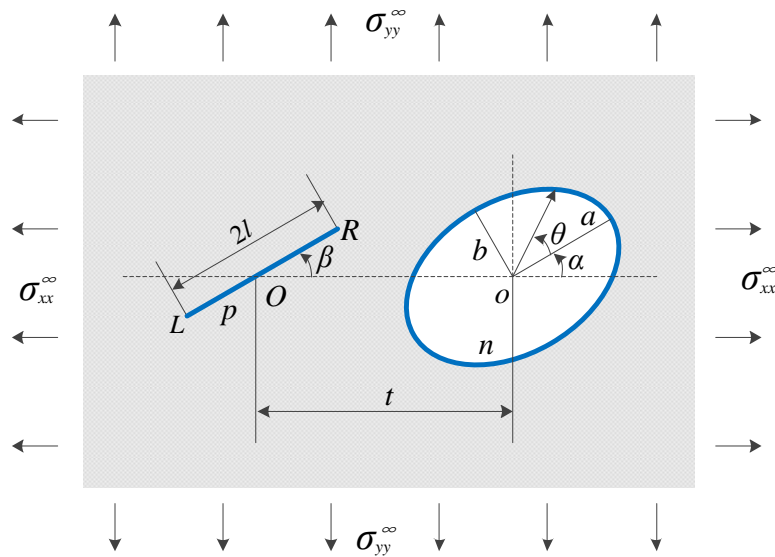


Figure 10: One elliptical-hole and one crack in an infinite elastic body subjected to far-field tensile stress and surface normal stresses on the elliptical-hole and crack.

at internal crack-tips L and external crack-tip R are analyzed under different loadings ($\sigma_{xx}^\infty/\sigma_{yy}^\infty, n, p$), geometries ($b/a, \alpha, \beta, t$) for providing some practical applications in engineering. For the purpose of convenience, the units of stress and distance are m and MPa , respectively. The investigations might be of great significance for practical engineering applications, where the proper shapes and locations of the holes can be used to promote or restrain crack propagation.

4.1 Effect of far-field stress ratio $\sigma_{xx}^\infty/\sigma_{yy}^\infty$

Fig. 11 plots interacting SIFs K_{IR}, K_{IIR} (solid line) and K_{IL}, K_{IIL} (dotted line) versus crack orientation angle β for various values of $\sigma_{xx}^\infty/\sigma_{yy}^\infty$ ($\sigma_{xx}^\infty/\sigma_{yy}^\infty = 0, 1, 2$) and t ($t = 3.4, 4, 5, \infty$), under $\sigma_{yy}^\infty = 1, n = p = 0$ (without any surface stresses), $a = 2, b = 1.6, l = 1, \alpha = 0^\circ$. It is worth noting that $t = \infty$ stands for the case of single crack (i.e., without elliptical-hole's effect). It is found from Fig. 11 that the curves of interacting SIFs versus crack orientation angle β at right crack-tip R ($K_{IR} - \beta, K_{IIR} - \beta$) have greater fluctuation than those at left crack-tip L ($K_{IL} - \beta, K_{IIL} - \beta$), since the elliptical-hole has stronger interference effect on the crack-tip nearby itself. It can be seen from $K_{IR} - \beta, K_{IL} - \beta$, curves (Figs. 11a), (c), (e)) that the locations of maximum K_{IR}, K_{IL} values are the same as the maximum K_I of single crack (i.e., $t = \infty$), differently from K_{IIR}, K_{IIL} (Figs. 11(b), (d), (f)). For example, when $\sigma_{xx}^\infty/\sigma_{yy}^\infty = 0$, the maximum values of K_{IR} and K_{IL} always appear at $\beta = 0^\circ$ for all of t , while the locations of maximum K_{IIR}, K_{IIL} are dependent of t . Decreasing t usually results in $K_{IR}, K_{IIR}, K_{IL}, K_{IIL}$ values away from those of single crack, since the closer to the crack the elliptical-hole, the stronger the interference influence (caused by elliptical-hole) is.

When $\sigma_{xx}^\infty/\sigma_{yy}^\infty = 0$ (Figs. 11(a)-(b)), interacting SIFs (except K_{IIL}) have greater values than the case of single crack for almost all of β , suggesting that crack is subjected to amplifying effect from the elliptical-hole. The amplifying effect increases when β and t decrease. As $\sigma_{xx}^\infty/\sigma_{yy}^\infty$ becomes larger ($\sigma_{xx}^\infty/\sigma_{yy}^\infty \geq 1$, Figs. 11(c)-(f)), there appears an intersection point between $K_{IR} - \beta, K_{IL} - \beta$ curves and $K_I - \beta$ curves (single crack), between $K_{IIR} - \beta$ curves and $K_{II} - \beta$ curves (single crack). Correspondingly, the orientation angle of crack is called as neutral orientation angle β_0 , in which the elliptical-hole has no influence on SIFs of crack-tips. When $0^\circ \leq \beta < \beta_0$ or $\beta_0 < \beta \leq 90^\circ$, the K_{IR}, K_{IIR}, K_{IL} have greater or smaller values than the case of single crack, manifesting that crack is subjected to amplifying or shielding effect from the elliptical-hole. In general, the shielding degree increases when β increases and t decreases. It can be also observed that increasing $\sigma_{xx}^\infty/\sigma_{yy}^\infty$ leads to decrease of β_0 of K_{IR}, K_{IL} and increase of shielding angle range ($\beta_0 < \beta \leq 90^\circ$), which benefits to the layout of stop-holes. Increasing t has significant influence on the degree of amplifying or shielding effect, but almost no influence on β_0 .

4.2 Effect of surface stresses n, p

Fig. 12 illustrates interacting SIFs K_{IR}, K_{IIR} (solid line) and K_{IL}, K_{IIL} (dotted line) versus crack orientation angle β for various values of n, p ($n = p = 0, n = -1, p = 0$, and $n = 0$,

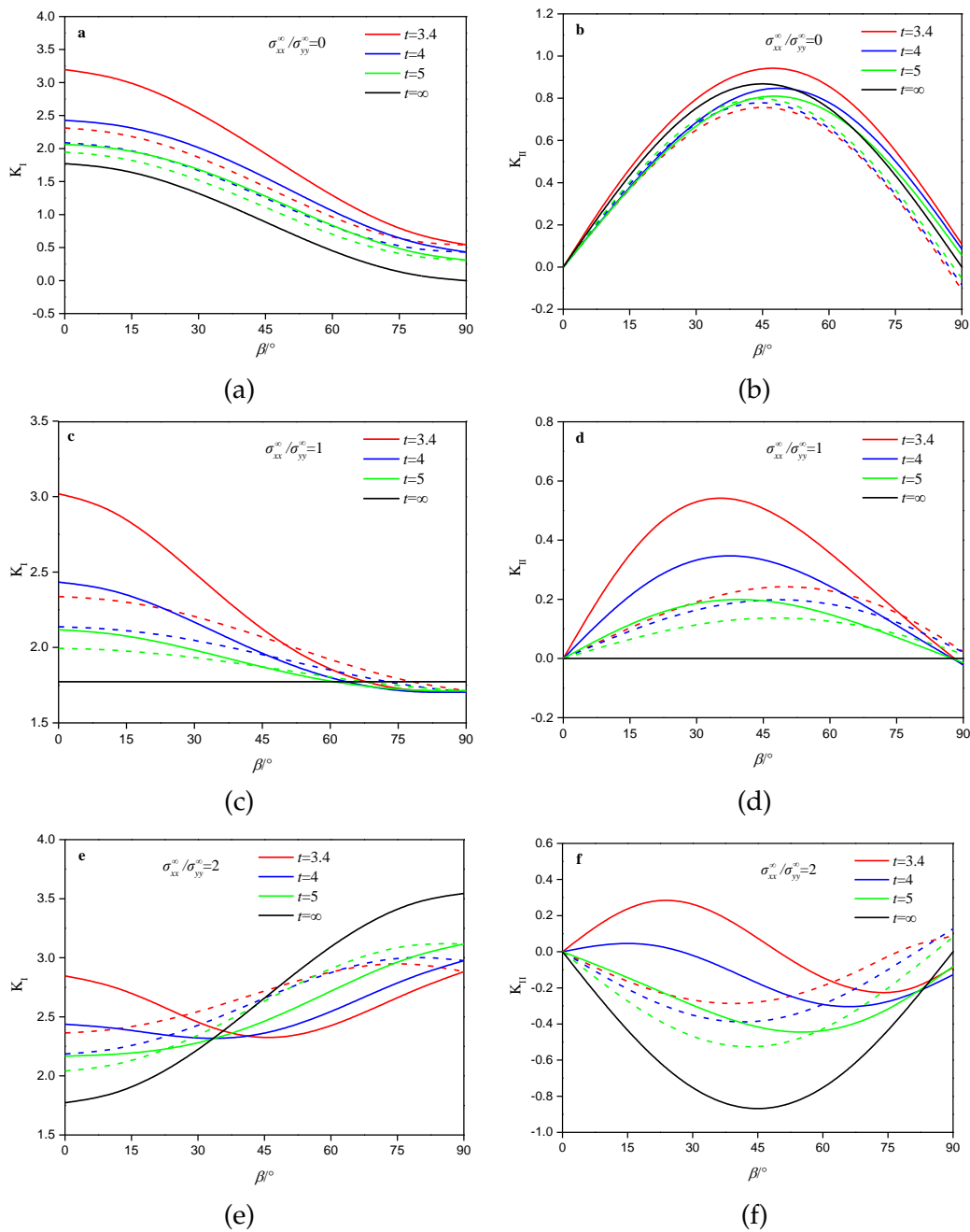


Figure 11: Interacting SIFs K_{IR} , K_{IIR} (solid line) and K_{IL} , K_{IIL} (dotted line) versus β for various values of $\sigma_{xx}^\infty/\sigma_{yy}^\infty$ and t ($\sigma_{yy}^\infty=1$, $n=0$, $p=0$, $a=2$, $b=1.6$, $l=1$, $\alpha=0^\circ$).

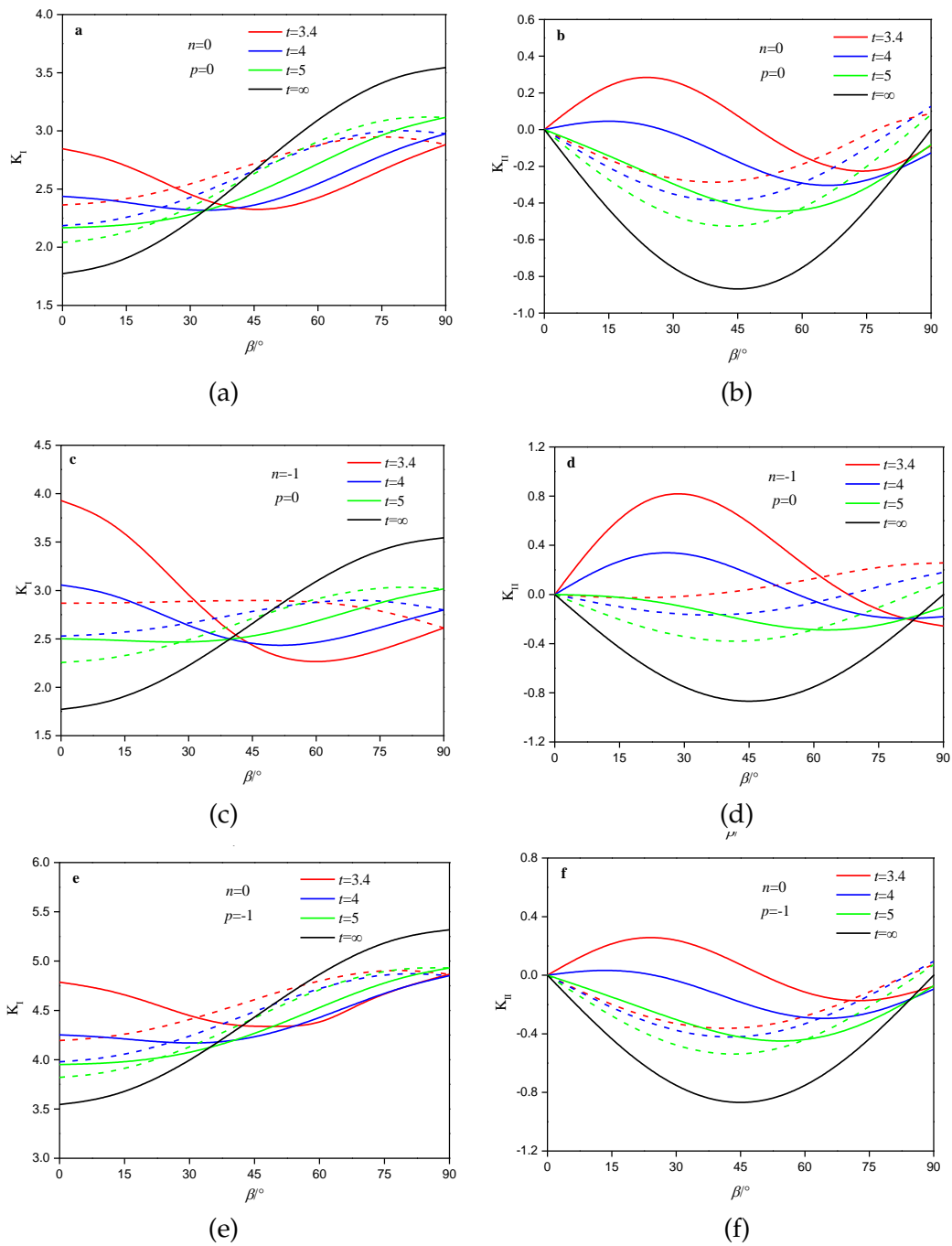


Figure 12: Interacting SIFs K_{IR} , K_{IIL} (solid line) and K_{IL} , K_{IIIL} (dotted line) versus β for various values of n , p and t ($\sigma_{xx}^\infty=2, \sigma_{yy}^\infty=1, a=2, b=1.6, l=1, \alpha=0^\circ$).

$p = -1$) and t ($t = 3.4, 4, 5, \infty$), under $\sigma_{xx}^{\infty} = 2$, $\sigma_{yy}^{\infty} = 1$ (i.e., $\sigma_{xx}^{\infty}/\sigma_{yy}^{\infty} = 2$, for obtaining the smaller β_0), $a = 2$, $b = 1.6$, $l = 1$, $\alpha = 0^\circ$. For clarity, Figs. 11(e)-(f) (i.e., $n = p = 0$) are again plotted in Figs. 12(a)-(b). As n changes from zero (Figs. 12(a)-(b)) to compressive stresses ($n = -1$, expanding the elliptical-hole, see Figs. 12(c)-(d)), almost all of maximum values of K_{IR} , K_{IIR} , K_{IL} , K_{IIL} are increased, suggesting that surface compressive stress on the elliptical-hole is helpful for crack initiation and propagation. Interestingly, the locations of maximum K_{IR} , K_{IL} values are changed from 90° to 0° for smaller t ($t = 3.4, 4$) with increasing n , differently from the case of far-field stresses (see Fig. 11). As p is varied from zero (Figs. 12(a)-(b)) to compressive stresses ($p = -1$, opening the crack, Figs. 12(e)-(f)), all of maximum values of K_{IR} , K_{IL} increase greatly, while the maximum K_{IIR} , K_{IIL} values have hardly change, since p mainly affect K_I but not K_{II} .

The neutral angle β_0 are also found between $K_{IR} - \beta$, $K_{IL} - \beta$ curves and $K_I - \beta$ curves (single crack), between $K_{IIR} - \beta$ curves and $K_{II} - \beta$ curves (single crack). Differently from the case of far-field stresses, n and p have almost no influence on β_0 . In addition, the holed-cracked distance have hardly influence on β_0 of K_{IR} , K_{IL} , K_{IIR} with the change in n , while increasing t results in the small increase of β_0 of K_{IR} , K_{IL} for all of p .

4.3 Effect of elliptical-hole size b/a

Fig. 13 shows interacting SIFs K_{IR} , K_{IIR} (solid line) and K_{IL} , K_{IIL} (dotted line) versus crack orientation angle β for various values of b/a ($b/a = 0.5, 0.8, 1$) and t ($t = 3.4, 4, 5, \infty$), under $\sigma_{xx}^{\infty} = 2$, $\sigma_{yy}^{\infty} = 1$, $n = p = 0$, $l = 1$, $\alpha = 0^\circ$. Note here that Figs. 13(c)-(d) are the same as Figs. 11(e)-(f). It can be seen that the $K_{IR} - \beta$, $K_{IIR} - \beta$, $K_{IL} - \beta$, $K_{IIL} - \beta$ curves is deviated from those of single crack as b/a is varied from 0.5 to 1 (i.e., circular-hole), indicating that the circular-hole has stronger interference influence on the crack than elliptical-hole. With the increase in b/a , the maximum K_{IR} , K_{IL} values decrease while the maximum K_{IIR} , K_{IIL} increase. Similar to surface stress applied on the elliptical-hole (Figs. 12(c)-(d)), the locations of maximum K_{IR} , K_{IL} values are changed from 90° to 0° for smaller t ($t = 3.4$) with increasing b/a . Moreover, when b/a is smaller ($b/a = 0.5$, Fig. 13(a)), t has almost no influence on the maximum K_{IR} , K_{IL} values. As b/a becomes larger (Figs. 13(c)-(f)), decreasing t usually leads to decrease of K_{IR} , K_{IL} and increase of K_{IIR} , K_{IIL} .

Similar to the case of far-field stresses, almost all of K_{IR} , K_{IIR} , K_{IL} , K_{IIL} are greater than those of single crack when $b/a = 0.5$ (Figs. 13(a)-(b)), indicating that the elliptical-hole has amplifying effect on crack, and amplifying effect decreases with increasing β and t . As b/a become larger, there appears an neutral crack orientation angle β_0 between $K_I - \beta$ curves of crack-tips R , L and single crack, between $K_{II} - \beta$ curves of crack-tips R and single crack. Increasing b/a leads to smaller β_0 of K_{IR} , K_{IL} and larger shielding angle range ($\beta_0 < \beta \leq 90^\circ$), while the β_0 of K_{IIR} , K_{IIL} is almost independent of b/a . Increasing t has significant influence on amplifying and shielding degree of K_{IR} , K_{IIR} , K_{IL} , K_{IIL} but almost no effect β_0 on and shielding angle range.

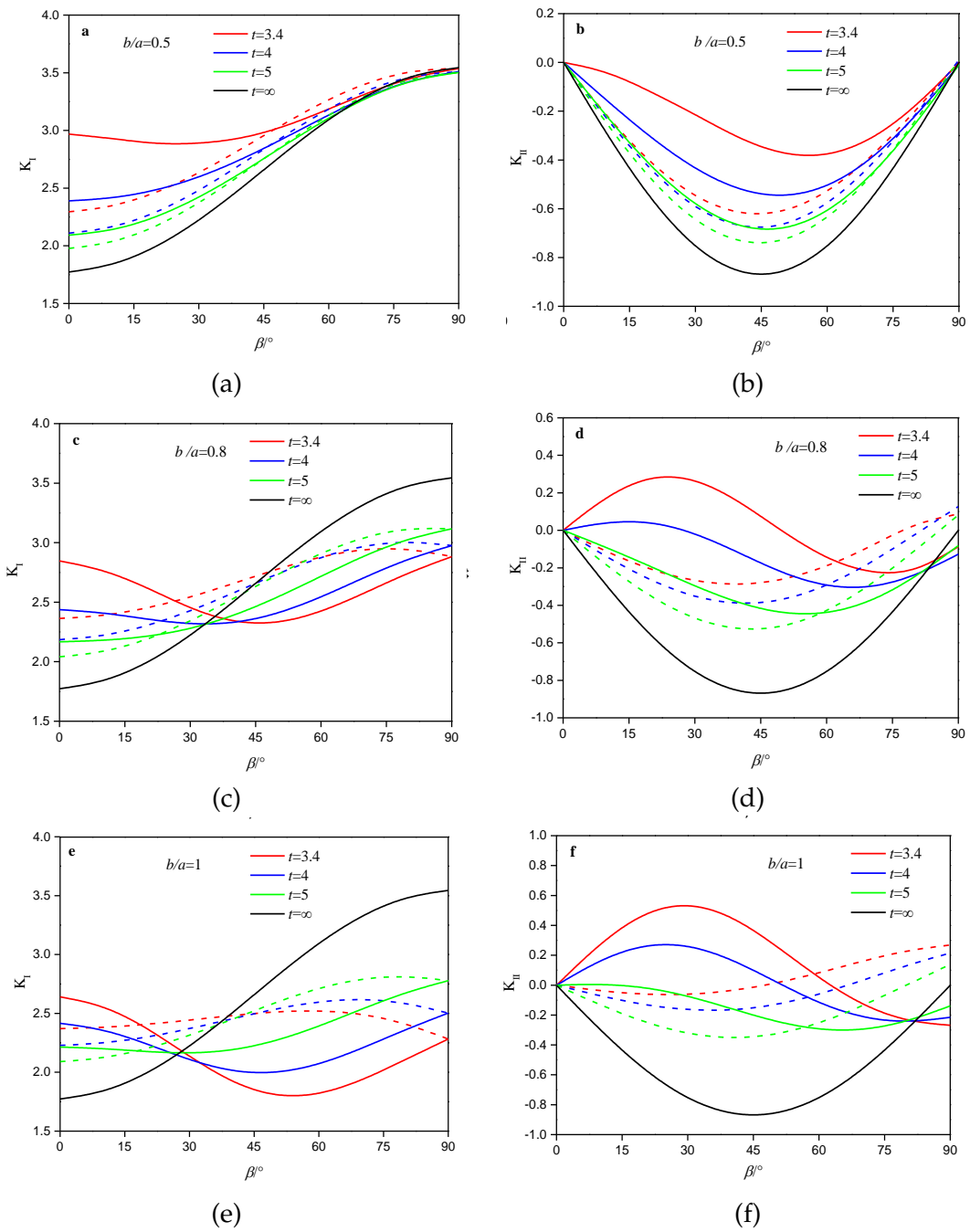


Figure 13: Interacting SIFs K_{IR} , K_{II} (solid line) and K_{IL} , K_{IIl} (dotted line) versus β for various values of b/a and t ($\sigma_{xx}^\infty = 2$, $\sigma_{yy}^\infty = 1$, $n = p = 0$, $l = 1$, $\alpha = 0^\circ$).

4.4 Effect of elliptical-hole orientation angle α

Fig. 14 presents interacting SIFs K_{IR} , K_{IIR} (solid line) and K_{IL} , K_{IIL} (dotted line) versus crack orientation angle β for various values of α ($\alpha = 0^\circ, 45^\circ, 90^\circ$) and t ($t = 3.4, 4, 5, \infty$), under $\sigma_{xx}^\infty = 2$, $\sigma_{yy}^\infty = 1$, $n = p = 0$, $l = 1$, Figs. 11(e)-(f) (i.e., $\alpha = 0^\circ$) are again presented in Figs. 14(a)-(b) for clarity. It can be found that as α is increased, the varying tendencies of $K_{IR}-\beta$, $K_{IIR}-\beta$, $K_{IL}-\beta$, $K_{IIL}-\beta$ curves have almost no change, and the maximum values of K_{IR} , K_{IL} have a slight decrease while the maximum values of K_{IIR} , K_{IIL} is gradually increased. As t is increased, the locations of maximum K_{IR} , K_{IL} values are changed from 0° to 90° for almost all of α . In addition, it can be observed that when $\alpha = 45^\circ$ (Figs. 14(c)), the K_{IR} and K_{IL} of $\beta = 90^\circ$ have different values, which is different from the above examples. This is because that the two crack-tips L and R are non-symmetric with the elliptical-hole.

For all of α , the neutral angle β_0 can be also found on the $K_{IR}-\beta$, $K_{IIR}-\beta$, $K_{IL}-\beta$ curves. Increasing ζ causes a little decrease of β_0 of K_{IR} , K_{IL} and amplifying angle range ($0^\circ \leq \beta < \beta_0$), while α has almost no influence on the β_0 of K_{IIR} (except $\alpha = 45^\circ$, Fig. 14d). Interestingly, there appear two neutral angles on the $K_{IIR}-\beta$ curve when $\alpha = 45^\circ$ (Fig. 14(d)), which is different from the above examples. In addition, it can be observed that when $\beta > 45^\circ$, the elliptical-hole always shields the K_{IR} , K_{IL} of crack-tips, which is basically irrelative to α .

From the above calculations and comparative analyses, it is verified that the new integral method has the advantages of simple form (without singularity), high accuracy and flexible loading conditions over current theoretical methods (e.g., Green's function method, displacement discontinuity method, singular integral equation method, pseudo-dislocations method) in calculating Mode I and Mode II SIFs of multiple elliptical-holes and cracks under both far-field and arbitrarily surface stresses. This new method can be further extended to calculate Mode III SIFs of multiple elliptical-holes and cracks under anti-plane stresses. Considering the elastic fundamental solutions and superposition principle, it is limited to linear elastic problem.

5 Conclusions

- (1) The exact fundamental stress solutions of single elliptical-hole under arbitrarily concentrated surface forces are derived based on Cauchy integral theorem to establish new integral equation formulations, which has the simpler formulation and higher calculation efficiency than those solved by Fourier series method. Accordingly, the new integral equation for the problem of multiple circular-holes and cracks can be developed for treating the more complicated problem of multiple elliptical-holes and cracks. No limitations are required on the sizes, number, locations and orientations of the elliptical-holes and cracks.
- (2) The new integral equation method is proved to be valid by comparing our solutions of interacting SIFs with those obtained by current theoretical and numerical

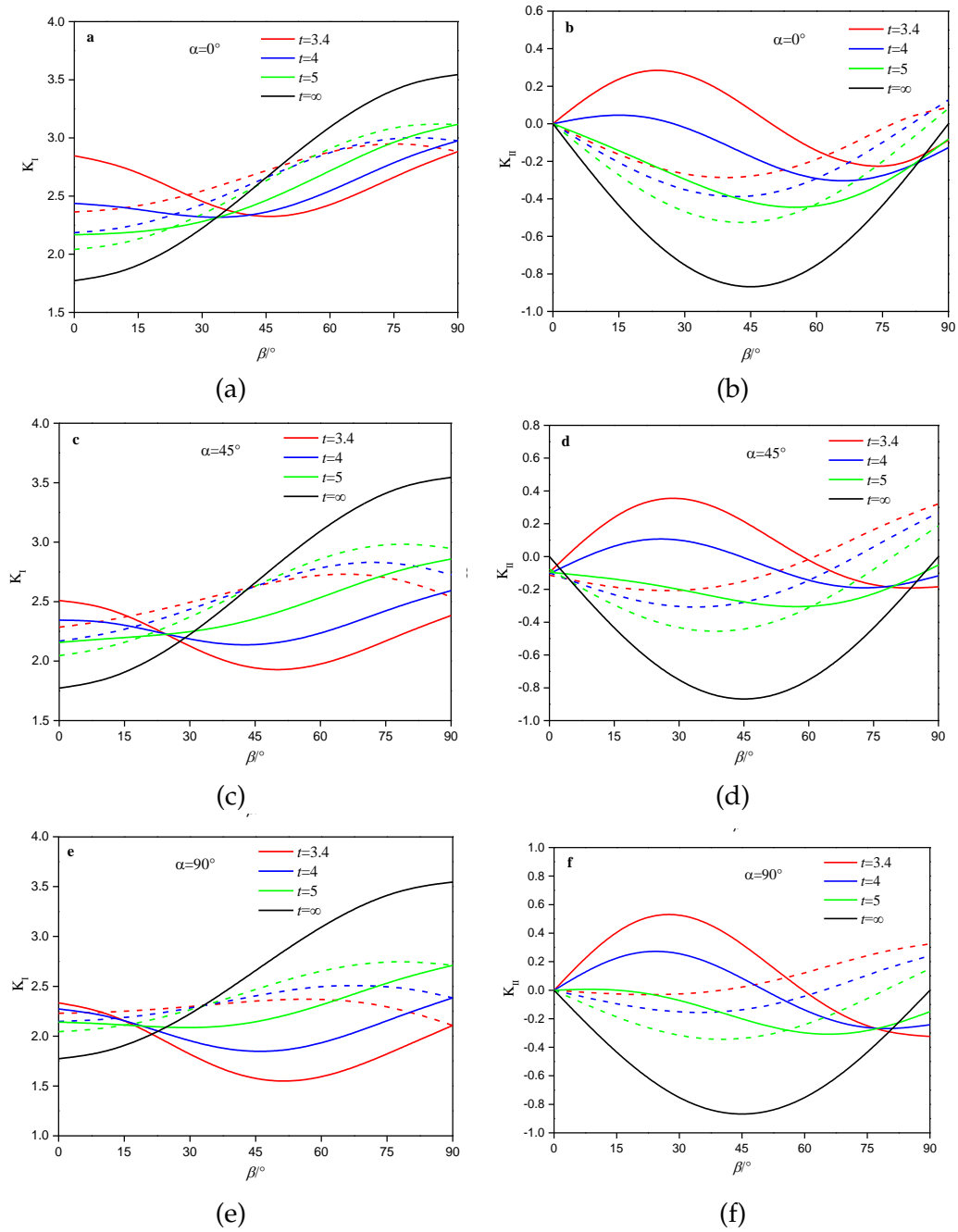


Figure 14: Interacting SIFs K_{IR} , K_{IIR} (solid line) and K_{IL} , K_{IIL} (dotted line) versus β for various values of α and t ($\sigma_{xx}^\infty = 2$, $\sigma_{yy}^\infty = 1$, $n = p = 0$, $a = 2$, $b = 1.6$, $l = 1$).

methods. It has simpler form (without singularity), higher accuracy (owing to exact fundamental stress solutions) and wider application (under both far-field stresses and arbitrary surface stresses) than the common methods. It can be further developed for the anisotropic problem of multiple holes and cracks.

- (3) For an infinite elastic body of one elliptical-hole and one crack under far-field biaxial stresses ($\sigma_{xx}^{\infty} \geq \sigma_{yy}^{\infty}$), there appears a neutral crack orientation angle β_0 (without elliptical-hole's effect) and the interacting SIFs of the crack-tip is amplified at $0 \leq \beta < \beta_0$ or shielded at $\beta_0 < \beta < 90^\circ$ by the elliptical-hole. The far-field stress ratio ($\sigma_{xx}^{\infty}/\sigma_{yy}^{\infty}$) and elliptical-hole size ($b/a \leq 1$) have significant influence on β_0 of K_I . Increasing $\sigma_{xx}^{\infty}/\sigma_{yy}^{\infty}$ and b/a (closer to 1, i.e., circular-hole) usually decreases β_0 of K_I and enlarges shielding angle range, which benefits to the layout of stop-holes.
- (4) The surface compressive stresses applied onto elliptical-hole (n) and crack (p) have great influence on interacting SIFs but not on β_0 . Increasing n and p usually results in increase of interacting SIFs and facilitates crack propagation and fracture networks. The elliptical-hole orientation angle (α) and holed-cracked distance (t) have great influence on the interacting SIFs while have little effect on β_0 . Increasing α usually leads to decrease of interacting SIFs and facilitates the crack-arrest. The smaller the t , the larger the effect of amplifying or shielding of interacting SIFs is.

Acknowledgements

The authors gratefully acknowledge the financial supports by National Natural Science Foundation of China (Nos. 51874351, 51474251 and 12072309) and Excellent Postdoctoral Innovative Talents Project of Hunan Province (No. 2020RC2001).

References

- [1] G. E. EXADAKTYLOS, AND M. C. STAVROPOULOU, *A closed-form elastic solution for stresses and displacements around tunnels*, Int. J. Rock Mech. Mining Sci., 39 (2002), pp. 905–916.
- [2] W. YI, Q. H. RAO, W. B. MA, D. L. SUN AND Q. Q. SHEN, *A new analytical-numerical method for calculating interacting stresses of multi-hole problem under both remote and arbitrary surface stresses*, Appl. Math. Mech., 41 (2020), pp. 1539–1560.
- [3] E. F. M. LETICIA, J. S. GABRIEL AND G. M. S. RAYMUNDO, *Study of geothermal water intrusion due to groundwater exploitation in the Puebla Valley aquifer system, Mexico*, Hydrogeology J., 14 (2006), pp. 1216–1230.
- [4] S. ALEVIZOS, T. POULET, M. SARI, M. LESUEUR, K. REGENAUER-LIEB AND M. VEVEAKIS, *A framework for fracture network formation in overpressurised impermeable shale: deformability versus diagenesis*, Rock Mech. Rock Eng., 50 (2017), pp. 689–703.
- [5] J. ZHANG, F. YANG, J. YANG, X. C. ZHENG AND F. X. ZENG, *Upper-bound stability analysis of dual unlined elliptical tunnels in cohesive-frictional soils*, Comput. Geotech., 80 (2016), pp. 283–289.

- [6] F. YANG, J. ZHANG, J. YANG, L. H. ZHAO, AND X. C. ZHENG, *Stability analysis of unlined elliptical tunnel using finite element upper-bound method with rigid translatory moving elements*, Tunnel. Underground Space Tech., 50 (2015), pp. 13–22.
- [7] S. C. GIANZERO, *Characteristic responses of resistivity tools in elliptical boreholes*, IEEE Transactions on Geoscience Electronics, 15 (2007), pp. 251–256.
- [8] D. GAO, Y. LIU, S. PAN, J. WANG AND X. M. ZHOU, *Longitudinal interference analysis of shale gas multi-stage fracturing horizontal wells upon high-precision pressure test*, Energy Sci. Eng., 8 (2020), pp. 2387–2401.
- [9] M. ISIDA, *Crack Tip Stress Intensity Factors for a Crack Approaching a Hole Centered on Its Plane*, Lehigh University, 1966.
- [10] M. ISIDA, *On the determination of stress intensity factors for some common structural problems*, Eng. Fracture Mech., 2 (1970), pp. 61–79.
- [11] F. ERDOGAN, G. D. GUPTA AND M. RATWANI, *Interaction between a circular inclusion and an arbitrarily oriented crack*, J. Appl. Mech., 41 (1975), pp. 1287–1297.
- [12] N. HASEBE, X. WANG AND M. KONDO, *Interaction between crack and arbitrarily shaped hole with stress and displacement boundaries*, Int. J. Fracture, 119 (2003), pp. 83–102.
- [13] V. J. C. NEWMAN, *Stress Analysis of Simply and Multiply Connected Regions Containing Cracks by the Method of Boundary Collocation*, Virginia Polytechnic Institute and State University, Blacksburg, 1969.
- [14] J. LEE AND A. MAL, *A volume integral equation technique for multiple inclusion and crack interaction problems*, J. Appl. Mech., 64 (1997), pp. 23–31.
- [15] K. X. HU, A. CHANDRA AND Y. HUANG, *Multiple void-crack interaction*, Int. J. Solids Structures, 30 (1993), pp. 1473–1489.
- [16] Y. B. WANG AND K. T. CHAU, *A new boundary element for plane elastic problems involving cracks and holes*, Int. J. Fracture, 87 (1997), pp. 1–20.
- [17] Y. B. WANG AND K. T. CHAU, *A new boundary element method for mixed boundary value problems involving cracks and holes: Interactions between rigid inclusions and cracks*, Int. J. Fracture, 110 (2001), pp. 387–406.
- [18] S. X. GONG AND S. A. MEGUID, *Microdefect interacting with a main crack: A general treatment*, Int. J. Mech. Sci., 34 (1992), pp. 933–945.
- [19] R. J. TANG, AND Y. B. WANG, *On the problem of crack system with an elliptic hole*, Acta Mech. Sinica, 1 (1986), pp. 47–57.
- [20] J. PU, *Effect of defective holes on crack using the boundary element method*, Eng. Anal. Boundary Elements, 30 (2006), pp. 577–581.
- [21] X. YAN, *An effective numerical approach for multiple void-crack interaction*, J. Appl. Mech., 73 (2006), pp. 525–536.
- [22] C. H. YANG AND A. K. SOH, *Modeling of voids/cracks and their interactions*, Theor. Appl. Fracture Mech., 38 (2002), pp. 81–101.
- [23] X. L. HAN, AND Z. Q. WANG, *Elastic fields of interacting elliptic inhomogeneities*, Int. J. Solids Structures, 36 (1999), pp. 4523–4541.
- [24] A. DEJOIE, S. G. MOGILEVSKAYA AND S. L. CROUCH, *A boundary integral method for multiple circular holes in an elastic half-plane*, Eng. Anal. Boundary Elements, 30 (2006), pp. 450–464.
- [25] R. R. BHARGAVA AND P. R. VERMA, *A study of crack-face boundary conditions for piezoelectric strip cut along two equal collinear cracks*, Adv. Appl. Math. Mech., 8 (2016), pp. 573–587.
- [26] W. YI, Q. H. RAO, S. LUO, Q. Q. SHEN, AND Z. LI, *A new integral equation method for calculating interacting stress intensity factor of multiple crack-hole problem*, Theor. Appl. Fracture Mech., 107 (2020), 102535.

- [27] N. I. MUSKHELISHVILI, *Some Basic Problems of the Mathematical Theory of Elasticity*, Netherlands: P Noordhoff, 1962.
- [28] Y. Z. CHEN, *General case of multiple crack problems in an infinite plate*, Eng. Fracture Mech., 20 (1984), pp. 591–596.
- [29] K. LANGE, *Numerical Analysis for Statisticians*, Springer, 2010.
- [30] T. KUNDU, *Fundamentals of Fracture Mechanics*, CRC Press, 2008.
- [31] B. KHOUYA, M. E. AMRANI AND M. SEID, *A Galerkin-characteristic finite element method for three-dimensional convection-dominated problems*, Adv. Appl. Math. Mech., 13 (2021), pp. 503–526.
- [32] K. P. JEOM, *The Nonlinear Finite Element Method*, John Wiley and Sons, New York, 2018.
- [33] YIRANG YUAN, HUAILING SONG, CHANGFENG LI AND TONGJUN SUN, *An upwind mixed finite element method on changing meshes for positive semi-definite oil-water displacement of darcy-forchheimer flow in porous media*, Adv. Appl. Math. Mech., 12 (2020), pp. 1196–1223.
- [34] K. J. BATHE, *Finite Element Method*, New Jersey: John Wiley and Sons Inc, 2000.
- [35] P. GUPTA, C. A. DUARTE AND A. DHANKHAR, *Accuracy and robustness of stress intensity factor extraction methods for the generalized/extended finite element method*, Eng. Fracture Mech., 179 (2017), pp. 120–153.